
J. Hass
J. M. Herrmann
T. Geisel

MPI for Dynamics and Self-Organization
Dept. for Nonlinear Dynamics
Bernstein Center for Computational
Neuroscience Göttingen, and
Institute for Nonlinear Dynamics
Georg-August-Universität Göttingen,
Bunsenstr. 10, 37073 Göttingen
joachim@nld.ds.mpg.de
michael@nld.ds.mpg.de
geisel@nld.ds.mpg.de

Optimal Mass Distribution for Passivity-Based Bipedal Robots

Abstract

This paper reports how and to what extent the mass distribution of a passive dynamic walker can be tuned to maximize walking speed and stability. An exploration of the complete parameter space of a bipedal walker is performed by numerical optimization, and optimal manifolds are found in terms of speed, the form of which can be explained by a physical analysis of step periods. Stability, quantified by the minimal basin of attraction, is also shown to be high along these manifolds, but with a maximum at only moderate speeds. Furthermore, it is examined how speed and stability change on different ground slopes. The observed dependence of the stability measure on the slope is consistent with the interpretation of the walking cycle as a feedback loop, which also provides an explanation for the destabilization of the gait at higher slopes. Regarding speed, an unexpected decrease at higher slopes is observed. This effect reveals another important feature of passive dynamic walking, a swing-back phase of the swing leg near the end of a step, which decreases walking speed on the one hand, but seems to be crucial for the stability of the gait on the other hand. In conclusion, maximal robustness and highest walking speed are shown to be partly conflicting objectives of optimization.

KEY WORDS—biped walking, passive dynamics, mass distribution, parametric optimization, walking speed, stability, minimal basin of attraction, feedback loop, swing-back phase

1. Introduction

Passive dynamic walking (McGeer 1990) has been developed as a conceptual alternative to trajectory-following methods in the design of bipedal robots and as a possible explanation for the efficiency of the human gait. The term refers to the capability of a mechanical device to walk stably on shallow downhill slopes without any actuation or control, powered only by gravity. Several experimental studies have shown that these kinds of walking machines work with reasonable stability over a range of slopes (McGeer 1990; Mayer et al. 2004; Collins et al. 2001), some of which showing a remarkable resemblance to the human gait. Moreover, there have been several attempts to construct actuated robots based on their passive dynamics (Collins et al. 2005; Ohta et al. 1999; Geng et al. 2006). In this way, the robot can walk on even ground and at a controlled speed while exploiting the benefits of its passive dynamics. A recent study (Collins et al. 2005) shows that these walkers efficiency is comparable to that of a human.

Given these results, it seems promising to apply the concept of passive dynamic walking in the design of autonomous robots used for operations in uneven terrain or entertainment purposes, or for intelligent leg prostheses. In all these cases, it is desirable to optimize certain gait characteristics, such as walking speed, energy efficiency or stability. A number of theoretical studies examined the effects of the hardware parameters on different gait characteristics (McGeer 1990; Garcia et al. 2000; Goswami et al. 1998; Coleman 1998). They showed that the passive gaits are quite robust against these changes and that several characteristics can be considerably influenced by the mass distribution. Garcia et al. (2000), for instance, managed to tune the mass distribution such that the robot could walk on arbitrarily low slopes, which corresponds

to optimal energy efficiency. However, all these explorations were performed one-dimensionally, varying only one parameter at a time with all others kept constant. A systematic numerical exploration of the entire multi-dimensional parameter space of a walker is a challenging task and has not been reported yet, except for a strongly simplified model, referred to as the “simplest walking model” (Garcia et al. 1998; Schwab and Wisse 2001). This straight-legged, planar device has a special mass distribution which allows for analytical solution of the equations of motion and leaves no free parameters but the slope. For this model, power consumption and basins of attraction have been extensively studied (Garcia et al. 1998; Schwab and Wisse 2001). It was found that these basins of attraction are very small and vanish completely for a slope of about 0.9° , where a period doubling bifurcation takes place and the period-one gait becomes unstable (Garcia et al. 1998; Goswami et al. 1998). This phenomenon is also observed in other models, but at different critical slopes. The physical mechanisms of this bifurcation, and those that maintain stability at lower slopes, are not fully understood, although it is known that the impacts of the feet on the ground provide a strong stabilizing effect (Hurmuzlu and Moskowitz 1987).

In this work, we study a straight-legged walking model in two dimensions with a continuous mass distribution, which is equivalent to that used in Coleman (1998). The objective of this study is twofold. On the one hand, we try to find mass distributions that optimize the passive gait in terms of walking speed and stability. On the other hand, we want to understand the physics of this simple system as thoroughly as possible to derive principles that are likely to be relevant also in more complex walking robots.

In the first part (Section 3), we aim to optimize the walker for speed. To explore the full six-dimensional parameter space in an efficient way, we employ a stochastic optimization algorithm. Walking speeds up to 1.84 m/s (about 2 leg lengths per second) are found along certain optimal manifolds in the subspace of hardware parameters. To understand the form of these manifolds and their change with ground slope, we conduct a physical analysis of one of the optimized walkers. The effect of the hardware parameters on two physical properties of the walker, the step period and the energy dissipation at heel-strike, is assessed while keeping initial conditions constant. In the second part (Section 4), we introduce a new measure for stability, the minimal basin of attraction, and examine the dependence of this measure on both the hardware parameters and the slope. It turns out that stability and walking speed are slightly conflicting demands, as the maximal-sized basins of attraction arise for parameter combinations with only moderate speed. We provide an explanation for this conflict by elaborating on the notion that the walking cycle can be interpreted as a feedback loop, which was introduced in Goswami et al. (1997) Finally (Section 5), we consider walking on slopes that are different from those the model was optimized for. The critical slope is shown to decrease with increasing walking

speed, consistent with the feedback loop interpretation. Moreover, we observe a decrease of speed at higher slopes, with was unexpected. Further analysis of the sample walker used in Section 3 reveals the existence of a swing-back phase of the swing leg near the end of each step, which is prolonged at higher slopes and results in reduced speed. This swing-back seems to be crucial for the stability of the “long-period” gait (Garcia et al. 1998), while the unstable “short-period” gait allows for a linear increase of walking speed with the slope.

2. Dynamical Walking Model

A passive walker can be modeled as an inverted multi-link pendulum (McGeer 1990; Garcia et al. 1998). The simplest version of such a model is the inverted double pendulum in two dimensions which resembles a walker with stiff knees (Garcia et al. 1998; Schwab and Wisse 2001). Figure 1 shows a sketch of the model. We consider symmetrical legs of mass m and length l . Their mass distribution is given by the vertical position of the center of mass c , a horizontal offset h , and the radius of gyration r_{gyr} , which defines the inertia by $I = mr_{\text{gyr}}^2$. We do not include an extra point mass at the hip to keep the number of parameters low, but its effect can be emulated by shifting up the center of mass and increasing the inertia appropriately. With these specifications, the model is equivalent to that used in Coleman (1998).

The walker is assumed to be fixed to the ground with the tip of its stance leg, so the dynamic variables are the angles between the links and the uninclined ground $\varphi = (\varphi_1, \varphi_2)$ and their respective angular velocities $\omega = (\omega_1, \omega_2)$. Each step starts from a double-stance configuration where the angles can be jointly expressed by the step distance σ between the legs. Initially, the walker is set into motion by some predefined angular velocities. The motion is governed by the equations

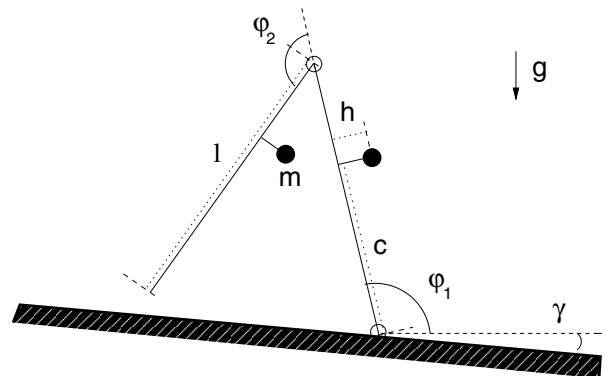


Fig. 1. Sketch of the walker on a downhill slope γ with variable and parameter conventions and the direction of gravity g .

of motion of the double pendulum until the free swing leg collides with the ground. These collisions (*heelstrikes*) are regarded as completely inelastic, instantly exchanging the role of the stance and the swing leg (Garcia et al. 1998). This results in dissipation of kinetic energy, which is compensated by gravitation in the passive gait. Heelstrikes are the only means of energy dissipation in this model, as we do not consider friction within the joints. Sliding motion of the swing leg when passing the stance leg is also ignored.

If the gait is periodic, the dynamical system formed by the equations of motion and the heelstrike transition rule exhibits a limit cycle. For convenient analysis, we define a Poincaré section at the instant after each heelstrike, following Garcia (1999). The mapping of the state (φ^n, ω^n) after the $(n - 1)$ th collision to the state $(\varphi^{n+1}, \omega^{n+1})$ after the n th collision is known as the *stride map* Ω (McGeer 1990). A periodic gait corresponds to a fixed point of Ω .

We construct the equations of motion for the smooth part of the cycle using the Lagrange formalism. This framework is convenient for the physical analysis in Section 3.3. In our coordinate system (cf., Fig. 1), the Lagrangian function of the double pendulum reads

$$\begin{aligned} \mathcal{L} &= \sum_{i=1}^2 \frac{m}{2} (\dot{x}_{ci}^2 + \dot{y}_{ci}^2) + \frac{I}{2} \omega_i^2 - mgy_{ci} \\ &= \frac{m}{2} [(c^2 + l^2)\omega_1^2 + (l - c)^2(\omega_1 + \omega_2)^2 \\ &\quad + 2l(l - c)\omega_1(\omega_1 + \omega_2)\cos\varphi_2^*] \\ &\quad + \frac{I}{2}(\omega_1^2 + (\omega_1 + \omega_2)^2) \\ &\quad - mg(c\sin\varphi_1^* + l\sin\varphi_1 + (l - c)\sin(\varphi_1 + \varphi_2^*)). \end{aligned} \quad (1)$$

The vector components (x_{ci}, y_{ci}) are the position of the i th center of mass measured from the contact point of the walker (cf., Fig. 1). The ‘*’ superscript denotes an angle modified to include the horizontal offset h in the following way

$$\begin{aligned} \varphi_1^* &= \varphi_1 + \arctan(h/c) \\ \varphi_2^* &= \varphi_2 - \arctan(h/c). \end{aligned} \quad (2)$$

The equations of motion follow from a modified version of the Euler–Lagrange equations (Hairer and Wanner 2002):

$$\begin{aligned} \mathbf{M} \cdot \ddot{\boldsymbol{\varphi}} &= \mathbf{f} \\ \text{with } \mathbf{M} &= \{M_{ij}\}, \quad \mathbf{f} = \{f_i\}, \quad \ddot{\boldsymbol{\varphi}} = \{\ddot{\varphi}_i\} \\ \text{and } M_{ij} &= \frac{\partial^2 \mathcal{L}}{\partial \dot{\varphi}_i \partial \dot{\varphi}_j}, \quad f_i = \frac{\partial \mathcal{L}}{\partial \varphi_i} - \sum_{j=1}^N \frac{\partial^2 \mathcal{L}}{\partial \dot{\varphi}_i \partial \varphi_j} \dot{\varphi}_j. \end{aligned} \quad (3)$$

With the Lagrange function eq. (1), eq. (3) yields

$$\begin{aligned} M_{11} &= m(c^2 + l^2 + (l - c)^2 + 2l(l - c)\cos\varphi_2^*) + 2I \\ M_{12} &= m(l - c)^2 + l(l - c)\cos\varphi_2^* + I \\ M_{21} &= m(l - c)^2 + l(l - c)\cos\varphi_2^* + I \\ M_{22} &= m(l - c)^2 + I \\ f_1 &= -mg(c\cos\varphi_1^* + l\cos\varphi_1 + (l - c)\cos(\varphi_1 + \varphi_2^*)) \\ &\quad + ml(l - c)\sin\varphi_2^*(2\omega_1\omega_2 + \omega_2^2) \\ f_2 &= -mg(l - c)\cos(\varphi_1 + \varphi_2^*) - ml(l - c)\omega_1^2\sin\varphi_2^*. \end{aligned} \quad (4)$$

At heelstrike, the roles of swing and stance leg are exchanged. The same equations can be used for the next step if the variables are also exchanged:

$$\begin{aligned} \varphi_1^+ &= \varphi_1^- + \varphi_2^- - \pi \\ \varphi_2^+ &= -\varphi_2^-, \end{aligned} \quad (5)$$

where the minus and plus sign represent quantities before and after the collision, respectively. The angular velocities after heelstrike are obtained from conservation of angular momentum around the new contact point $H_{cp}^+ = H_{cp}^-$ and the hip connection $H_{hp}^+ = H_{hp}^-$ (cf., Figure 1) (Garcia 1999).

For the optimization and analysis of the walker in the following, we consider the mass m and length l of the legs, the positions of their centers of mass given by c and h and the joint radius of gyration r_{gyr} . However, changing the masses and lengths of both legs by the same amount does not qualitatively change the dynamics, because all terms of the Lagrangian eq. (1) scale with the same order of m and l . Thus, we fix the mass at 30 kg and length at 0.9 m for each leg. This restricts the free hardware parameters to c , h and r_{gyr} .

3. Optimization of Walking Speed

The initial step length σ , the angular velocities ω_1, ω_2 and the three hardware parameters form a six-dimensional parameter space. To explore this space in an efficient way, we formulate the problem as a numerical optimization task.

3.1. Optimization Method and Fitness Function

The performance of each set of parameters is assessed by the fitness function f which is evaluated after a walking simulation of 10s:

$$\begin{aligned} f &= S \times \exp(-(\Delta/\delta)^2) \times P(\sigma, \sigma_{\min}) \\ \text{with } P(\sigma, \sigma_{\min}) &= \begin{cases} \sigma_{\min}/\sigma & \text{if } \sigma_{\min} < \sigma \\ 1 & \text{otherwise} \end{cases}. \end{aligned} \quad (6)$$

S marks the number of steps the walker takes during this time as a measure of the walking speed. Δ is the largest deviation

of the angles and angular velocities between two successive steps. The squared exponential dependence with a small scale constant δ ensures that the initial conditions stay within a small neighborhood of a fixed point for high-fitness solutions. This resembles the definition of Lyapunov stability. Finally, $P(\sigma, \sigma_{\min})$ is a penalty function that reduces the fitness by σ_{\min}/σ if the smallest step length σ_{\min} of the walker falls below the initial step length σ at any time of the simulation. This is necessary because the walker tends to prefer gaits with step lengths that are far too small to be realistic (cf. Mayer et al. 2004). The penalty does not prevent small σ being selected for initial conditions, but it does prevent convergence to a periodic gait with excessively small σ_{\min} . This precaution turns out to be sufficient.

For optimization, we use a technique called NPOSA (new population-oriented simulated annealing) (Cho et al. 1998), which combines the paradigms of simulated annealing and genetic algorithms. Due to the stochastic nature of the algorithm, we obtain a population of parameter sets with a wide range of fitness values, rather than one optimal solution per trial. This allows us to analyze the dependence of the fitness on the mass distribution and initial conditions. Furthermore, regions of high fitness will be covered by many solutions, while low-fitness regions remain sparse. Thus, a more thorough analysis of the interesting parameter regions is possible.

We apply the optimization method independently for different downhill slopes ranging from 0.0001° to 15° . After the optimization, the parameter combinations are used as initial values for Newton's method and a subsequent linear stability analysis to label each set as either 'stable fixed point', 'unstable fixed point' or 'no fixed point'. Note that this kind of analysis is not performed during the optimization itself to promote computational efficiency. However, the majority of parameter combinations are close to fixed points as a result of the optimization. Stable fixed points are found over a broad range of parameters at all slopes up to 10° . We restrict further analysis to optimized slopes between 1 and 10° for clarity of display. It turns out that, as expected, high fitness values correspond to high walking speed (cf., Fig. 10 for the range of speeds as a function of γ).

3.2. Constraints on Successful Parameters

Plotting the subspace of c and r_{gyr} after optimization reveals a cluster region of solutions near the point $(c, r_{\text{gyr}}) = (l, 0)$, which we call the "singular limit" (cf., Section 3.3), and a circular-shaped preferred manifold (Figure 2, upper panel). Both regions can be defined by their fitness, which is maximal in the cluster region, decreases with distance from the singular limit, and stays relatively high within the preferred manifold compared to its surroundings. However, there is a small offset both from $c = l$ and $r = 0$ which automatically emerged from the demands on performance. The distribution of parameters looks similar for all slopes, but the radii of the preferred man-

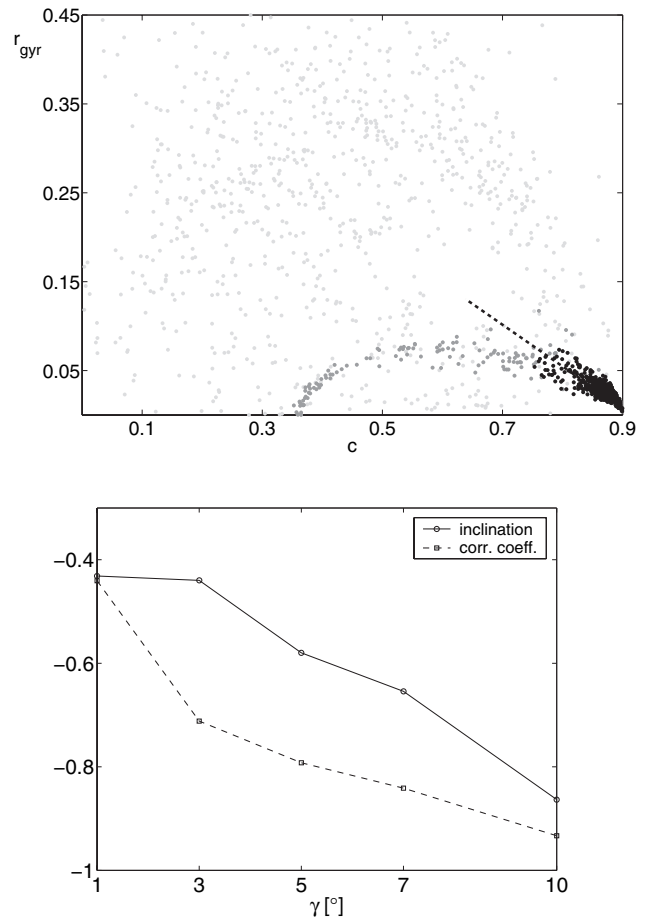


Fig. 2. (Upper panel) Mass distribution (with h fixed to 0) leading to stable fixed points of the stride map $\gamma = 5^\circ$. The successful sets scatter over the whole space, but there is a cluster region near the singular limit ($f > 25$, black dots) and a circular-shaped preferred manifold ($f > 19$, dark grey dots). The dotted line shows the linear fit to the preferred manifold within the cluster region. (Lower panel) Inclination with respect to the c -axis (solid line) and correlation coefficient (dotted line) of the linear approximation of the points within the cluster region for each slope.

ifolds increase with the slope. This can be shown by fitting the relation between c and r_{gyr} within the cluster region with a linear function (dotted line). The cluster region is arbitrarily defined by the intervals $c \in [0.8, 0.9]$ and $r_{\text{gyr}} \in [0, 0.06]$ for this purpose. In Figure 2 (lower panel), one sees that this correlation is tightened and the negative inclination of the fit with respect to the c -axis increases with the slope. The initial conditions within the cluster region also exhibit clear correla-

tions between each other. A 3D plot reveals smooth surfaces resembling hyperbolic paraboloids that are distinct for different slopes (Figure 3). While the increase in the step length σ with γ is most clearly visible in the figure, both angular velocities also increase, ω_2 much more than ω_1 . Note that there is only one stable fixed point for a given hardware configuration, so each of the points in Figure 3 corresponds to a distinct mass distribution.

The results discussed above are independent of whether h is used as an optimized parameter or set to zero. If h is optimized, its variance is relatively small compared to c and r_{gyr} and its mean decreases to negative values at higher slopes (Figure 4). That reflects a tendency to shift the overall center of mass of the walker backwards at higher slopes.

3.3. Physical Effects of the Mass Distribution

To understand the effects observed in Section 3.2, we study a sample walker with parameters drawn from the cluster region at $\gamma = 5^\circ$, which are listed in Table 1. We assess the influence of c and r_{gyr} on two important dynamic parameters, the period and the energy dissipation at heelstrike, while the initial conditions and h are kept fixed to the long-period solution (for a discussion of the short-period gait, cf., Section 5). The horizontal offset h influences the dynamics in a more global way which is discussed at the end of this section.

The period T is defined as the first time at which the walker reaches a double-stance position that is geometrically identical with the initial position. From geometry (Figure 1), one can see that this is the case if the conditions

$$\varphi_1(T) = \varphi_1(0) + \varphi_2(0) - \pi \quad (7)$$

and

$$\varphi_2(T) = -\varphi_2(0) \quad (8)$$

are fulfilled at the same time T . Values at time zero correspond to the initial conditions at the beginning of a step.

We first consider each leg as a single physical pendulum that is fixed at its respective connection point. In this case, the equations of motion eq. (3) and (4) reduce to

$$m(c^2 + r_{\text{gyr}}^2)\ddot{\varphi}_1 = -mgc \cos \varphi_1^* \quad (9)$$

for the stance leg. Furthermore, the kinetic and the potential energy are given by

$$\begin{aligned} E_{\text{kin}} &= \frac{m}{2}(c^2 + r_{\text{gyr}}^2)\dot{\varphi}_1^2 \\ E_{\text{pot}} &= -mgc \sin \varphi_1^*. \end{aligned} \quad (10)$$

The equations for the swing leg have the same form if c is replaced by $(l - c)$, and the sum $\varphi_1 + \varphi_2^*$ and its derivatives are used instead of φ_1^* . However, the dynamics of stance and swing leg are quite different. The stance leg, as an inverted

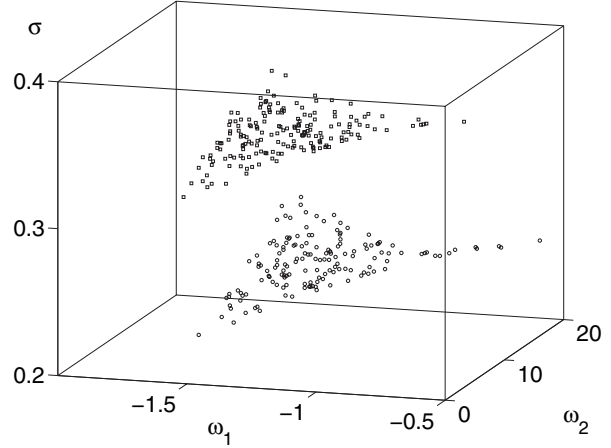


Fig. 3. The three initial conditions form smooth surfaces for stable solutions inside the cluster region. Only the initial conditions at $\gamma = 3^\circ$ (circles) and $\gamma = 5^\circ$ (squares) are shown for clarity.

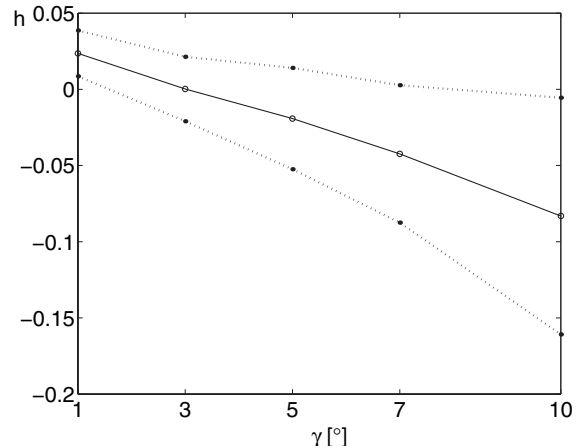


Fig. 4. Mean and standard deviation range of h as a function of the slope.

pendulum, uses the initial kinetic energy to rise to its apex position $\varphi_1 = \pi/2$, where the maximal potential energy is reached. If the kinetic energy is lower than the difference between the initial and maximal potential energy, the leg does not reach the apex at all and falls backwards. Therefore, the period of the leg is dominated by the amount of initial kinetic energy. The swing leg, on the other hand, reaches the position defined by eq. (8) even if $E_{\text{kin}}(0) = 0$, so the period of the leg is affected more by its dynamics. In particular, for $c \rightarrow l$ and

Table 1. Parameters of the Sample Walker at $\gamma = 5^\circ$.

| Mass Distribution | $c = 0.820$ | $r_{\text{gyr}} = 0.113$ | $h = 0$ |
|-----------------------------------|------------------|--------------------------|--------------------|
| Initial conditions (long-period) | $\sigma = 0.467$ | $\omega_1 = -1.069$ | $\omega_2 = 2.034$ |
| Initial conditions (short-period) | $\sigma = 0.476$ | $\omega_1 = -1.577$ | $\omega_2 = 1.634$ |

$r_{\text{gyr}} \rightarrow 0$, the angular acceleration diverges and T approaches zero. Therefore, we call the point $(c, r_{\text{gyr}}) = (l, 0)$ the *singular limit*. In Figure 5, the dependence of T on c and r_{gyr} is shown for both legs. The semi-circular isoclines in T are due to the quadratic terms in E_{kin} , and the equation of motion for the stance and swing leg, respectively.

Now we discuss the period of the whole walker as defined by the equation in Section 2 (Figure 6, upper panel). Here, the period is defined as the moment of the first heelstrike. Interestingly, one sees that the gross structure of Figure 5 (lower panel) is reproduced near the singular limit, which means that the nonlinear effects are weak in this region and the dynamics of the walker is dominated by the dynamics of the swing leg. Moreover, it turns out that only for a small fraction of the hardware parameters, the moment of the heelstrike coincides with the periods of both of the legs (black line).

The other dynamic parameter, the energy dissipation, is defined by

$$\delta E := \frac{E_{\text{kin}}^- - E_{\text{kin}}^+}{E_{\text{kin}}^-} = 1 - \frac{E_{\text{kin}}^+}{E_{\text{kin}}^-}. \quad (11)$$

This parameter jointly depends on the mass distribution, the angles and angular velocities at the instant of the heelstrike, and on E_{kin} itself. Consequently, the dependence of δE on c and r_{gyr} is a complex one (Figure 6, upper panel). However, very close to the singular condition, this dependence is similar to that of T in Figure 6 (lower panel).

Note that the numerical values of T and δE as well as the size of the admissible areas in Figure 6 are specific to the chosen initial conditions and the slope. However, the form of the isoclines in the hardware parameter space is qualitatively independent of these specifications. For any admissible combination of initial conditions, there is a submanifold in the space of c and r_{gyr} for which the periods of the pendula coincide. Out of these possible hardware configurations, those will lead to a fixed point which also provide the right amount of δE to restore the initial angular velocities.

Based on the analysis above, we can explain some of the optimization results in Section 3.2. The cluster region arises due to the dense packing of isoclines near the singular limit (Figure 6), such that only a slight variation in c or r_{gyr} makes the parameter combination fit to a wide range of initial conditions. Moreover, the period T is low near the limit, so the speed of any successful walker is high. Near the cluster region, we can also explain the form of the manifolds. Comparing Figure 2 (lower panel) with Figure 6, one sees that for higher

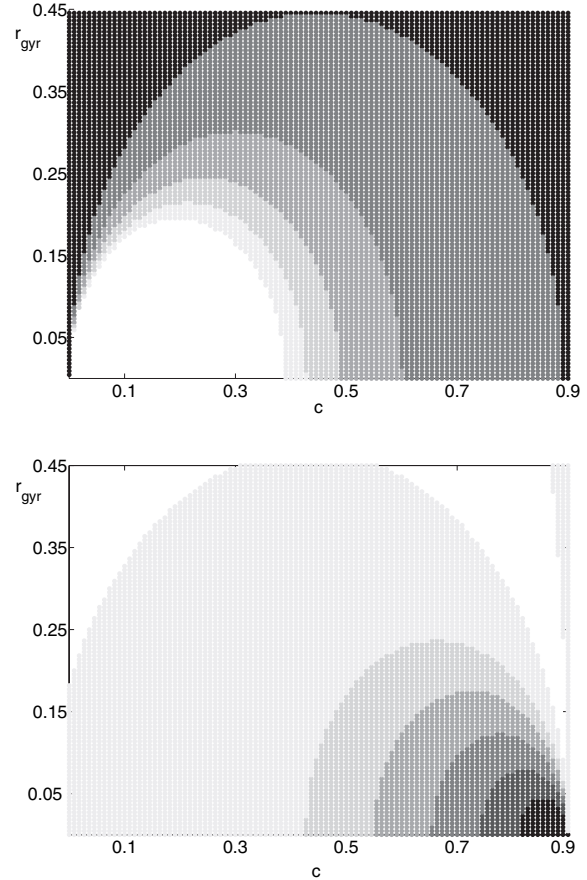


Fig. 5. Period T of the stance leg (upper panel) and the swing leg (lower panel) as single pendula and dependence on c and r_{gyr} . The shading represents different intervals of T from low (black) to high (light grey), so the borders between the shaded areas play the role of T isoclines. T is increased by 0.03 for the stance leg and by 0.1 for the swing leg within each of the areas.

slopes, parameter regions with higher values of δE are preferred. This is consistent with the increase of energy available at higher slopes, which must be matched by increasing dissipation as well to result in a periodic gait (cf., Section 4.2). However, this choice of parameters also implies a slower gait, as the period T increases (cf., Section 5).

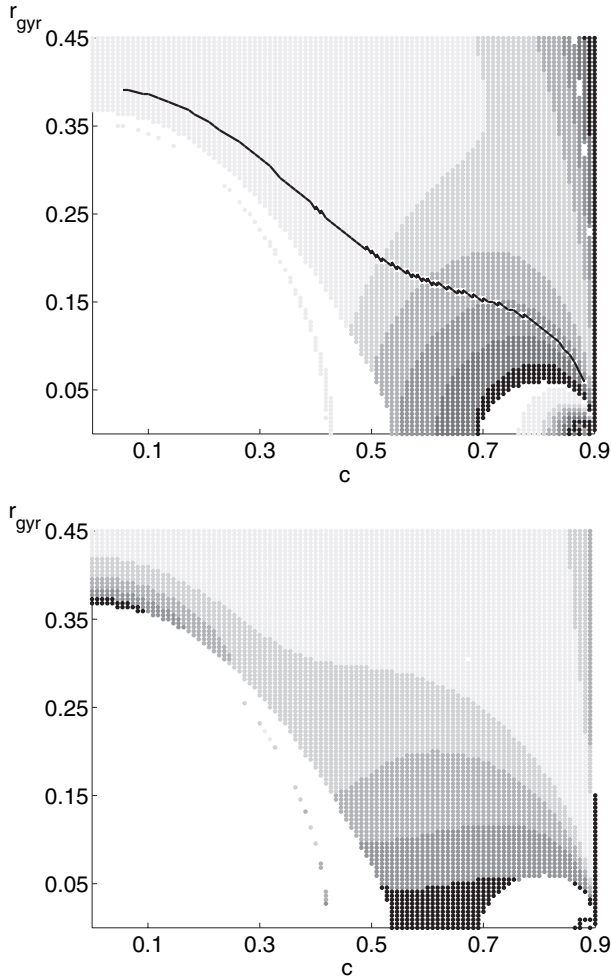


Fig. 6. Period T of the walker (upper panel) and energy dissipation δE at heelstrike (lower panel) and dependence on c and r_{gyr} . The shading represents different intervals of T and δE , respectively. T is increased by 0.05 and δE is increased by 0.2 within each of the areas. For the black line in the left figure, the periods of the walker and both legs coincide, which is a necessary conditions of a fixed point of the stride map Ω .

Finally, we discuss the effect of the parameter h on the dynamics of the walker. Consider a positive value of h . The center of mass of the stance leg is shifted upwards in this case (cf., Figure 1), increasing the available potential energy. This can also be seen in eq. (3). Conversely, for the swing leg the center of mass is lowered and the potential energy is decreased. Thus, for a walker within the cluster region, a positive h leads to a net increase of potential energy and a negative value to a net decrease. In the context of Section 3.2, it seems that h is chosen to increase the potential energy at low slopes and to decrease it at higher slopes. This behavior can be understood in terms of stability and is discussed in the next section.

4. Stability Against Perturbations and Parametric Changes

4.1. Minimal Basin of Attraction

The fitness function eq. (6) does not contain a measure for stability. In this section, we introduce such a measure and examine how it relates to walking speed. Stability is usually quantified either by basins of attraction, or by the eigenvalues of the Jacobian of the stride map. The first corresponds to the size of a perturbation one can apply to the initial conditions of a fixed point while maintaining convergence, while the latter assumes infinitesimally small perturbations and quantifies the convergence time. To combine these spatial and temporal aspects, we compute basins of attraction on the basis of the convergence time: if a set of initial conditions falls into a small neighborhood of the fixed point within a defined number of steps, it is included in the basin. An example of a basin for a maximum of 3, 10 and 50 steps, respectively, is shown in Figure 7. One sees that the basin size strongly depends on the demanded convergence time. We use 50 steps in the following. To calculate the basin size for all of the fixed points in an efficient way, we use an algorithm that starts testing at the unperturbed initial conditions $(\sigma, \omega_1, \omega_2)$ and applies increasing values of perturbation in each iteration. For the n th iteration,

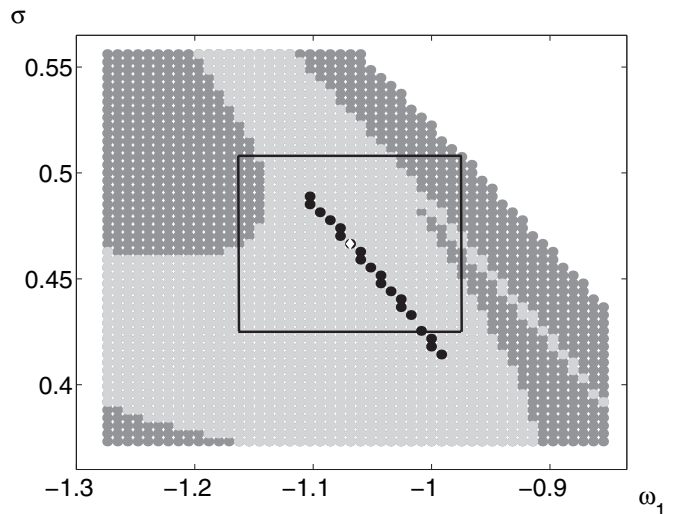


Fig. 7. Section from the basin of attraction for one of the fixed points at $\gamma = 5^\circ$. The shading marks the number of steps the walker takes until the initial conditions fall into a small neighborhood of the fixed point: less than 50 steps (dark gray), less than 10 steps (light gray) or less than three steps (black). The unperturbed initial conditions are depicted as a white diamond in the middle, and the minimal basin of attraction (see text) is shown as a black frame.

the perturbed initial condition are defined as

$$\begin{pmatrix} \sigma \\ \omega_1 \\ \omega_2 \end{pmatrix}_n \in \begin{bmatrix} \sigma - n \Delta\sigma, & \sigma + n \Delta\sigma \\ \omega_1 - n \Delta\omega_1, & \omega_1 + n \Delta\omega_1 \\ \omega_2 - n \Delta\omega_2, & \omega_2 + n \Delta\omega_2 \end{bmatrix}, \quad (12)$$

where $\Delta\sigma$, $\Delta\omega_1$ and $\Delta\omega_2$ are different scale factors that are chosen by experience such that the number of points inside a typical basin of attraction is approximately equal in each direction. The number of points tested in the n th step is thus n^3 , forming a cuboid around the fixed point in the space of initial conditions with different edge lengths set by the scale factors. If all of the points inside a cuboid are tested positive, this cuboid is said to belong to the *minimal basin of attraction*, which is in turn defined by the largest cuboid included. The volume index of this cuboid is denoted with n_{\min} . For illustration, the minimal basin of attraction is depicted as a black frame in Figure 7. Although the calculation of n_{\min} omits a number of points that are contained in the full basin, we find that the qualitative behavior of both measures is identical (Figure 8, upper panel). Furthermore, n_{\min} has the advantage of being insensitive to which of the variables a perturbation is applied to. If, for example, the basin is large in the direction of σ , but small for ω_1 , the total size of the basin may still be high, although a small perturbation in ω_1 may cause the walker to fall. Using n_{\min} as a stability measure avoids these problems.

In Figure 8 (upper panel), we plot n_{\min} and the scaled total basin size against walking speed at $\gamma = 5^\circ$. The situation is similar to the other slopes. It is apparent that the basin size is maximal at parameters and initial conditions that result in moderately high, but not the highest, speed. Thus, maximal stability and maximal walking speed seem to be antagonistic demands. Furthermore, we examine the dependence of n_{\min} on the slope (Figure 8, lower panel). In contrast to previous results on the simplest walking model (Schwab and Wisse 2001), we find that there is a maximum of stability at medium slopes and a decrease both to higher and lower slopes.

4.2. The Walking Cycle as a Feedback Loop

While we cannot provide a full analysis of the mechanism that stabilizes the walker, we offer a conceptual framework that helps to qualitatively understand several stability issues, which are otherwise illusive. It has been argued by Goswami et al. (1997) that a periodic gait arises due to a feedback-type mechanism in kinetic energy. During the swing phase, kinetic energy increases by ΔE due to the transformation of potential energy. If there were no energy dissipation at the heelstrike, this increase would be continued in each step without any bound. A limit cycle can only arise if ΔE and the loss of energy δE due to the heelstrike are balanced. Thus, in terms of control theory, the swing phase can be seen as a disturbance in the net kinetic energy, and the heelstrike as a feedback controller that compensates for this disturbance.

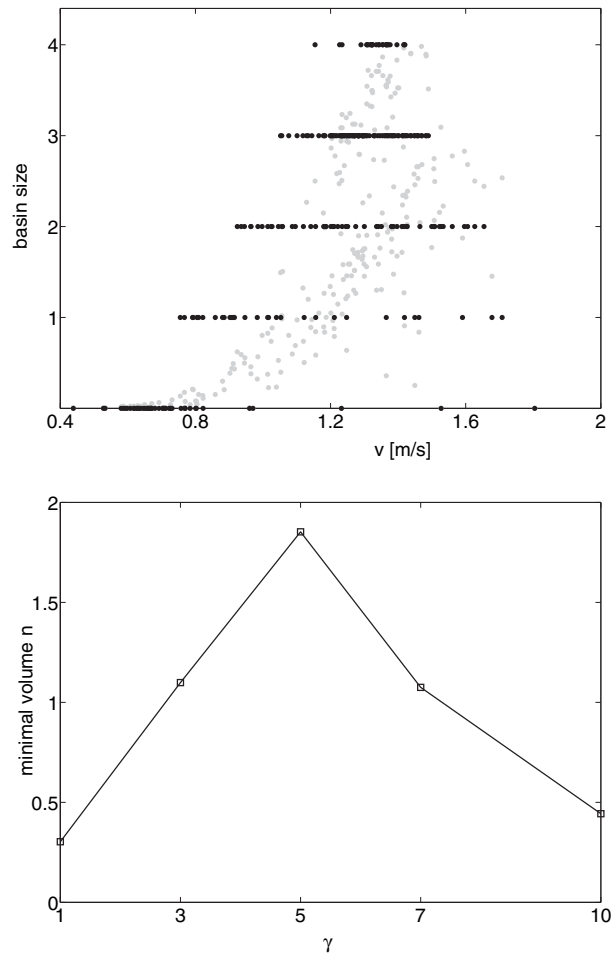


Fig. 8. (Upper panel) Volume parameter n of the basins of attraction as a function of the walking speed v for all stable solutions at $\gamma = 5^\circ$ (black dots) and the full basin size scaled to the maximal value of n for comparison (grey dots). (Lower panel) n as a function of the slope γ . n is averaged over the population of stable solutions for each slope.

Now consider a change in the initial conditions such that the balance is disturbed by ϵ . The heelstrike evokes a reaction that is directed to compensate for this disturbance, i.e., ΔE is increased in the next step if ϵ was negative, or increased if it was positive. The magnitude of this reaction increases with δE , so we argue that δE acts as the controller gain of a feedback controller that stabilizes the gait.

Within this framework, we can study the decay time of a perturbation ϵ and the eigenvalues of the Jacobian of the stride map Ω in dependence on γ , using again the sample walker defined in Section 3.3 (Figure 9). If the dissipation is low, as for small γ , the compensatory effect of the heelstrike

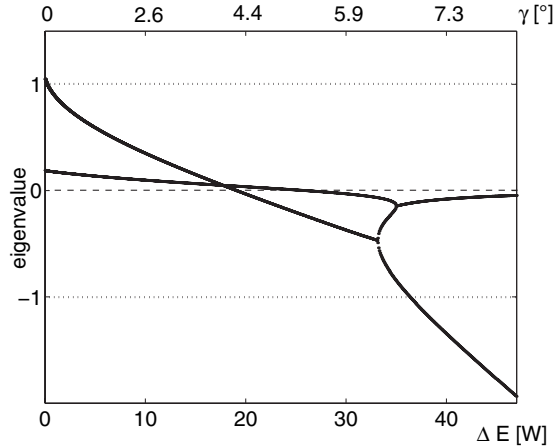


Fig. 9. Eigenvalues of the Jacobian of the stride map Ω as a function of the kinetic energy increase ΔE during the swing phase. The parameters and initial conditions for $\gamma = 5^\circ$ are the same as in Section 3.3.

is relatively weak. The decay of the perturbation is slow, and for very small δE , it is even possible that the corresponding fixed point is unstable. This is reflected by the fact that the eigenvalue of greatest absolute value is around one for low slopes. As ΔE and δE increase, the perturbation decays faster and the eigenvalue decreases, up to the point where the compensation becomes greater than the actual perturbation, which leads to an alternating sign in the perturbation in each step and a negative sign of the eigenvalue. For even higher ΔE , the eigenvalue approaches -1 and the decay of the perturbation takes the form of a damped oscillation, with its damping constant decreasing as δE increases. As soon as the eigenvalue crosses -1 , this oscillation is not damped any more and a stable limit cycle arises between two energetic states above and below the fixed point. Oscillations and instability at high gains are well-known phenomena in feedback controllers (Lewis 2002).

This analysis explains the dependence of the minimal basin of attraction size on the slope, as the decay time of a perturbation increases both for high and low slopes, such that the basin size decreases. However, it also shows that stability actually depends on the values of ΔE and δE , rather than on the slope itself. This is illustrated by the behavior of h that was found in Section 3.2: h is modified such that ΔE is increased for low slopes and decreased at higher slopes. In each case, stability increases compared to $h = 0$. The conflict between stability and walking speed can be understood in the same way. Maximal speed corresponds to a high value of ΔE with lower stability, whereas some intermediate value of ΔE at a moderate speed corresponds to the zero crossing of the eigenvalues and maximal stability.

5. Walking on Different Slopes

Besides the initial conditions and the mass distribution, the most frequently varied parameter is the slope γ . It has been shown in several studies that a passive walker can be used on a range of slopes if the initial conditions are adapted in a continuous way (McGeer 1990; Garcia et al. 1998). While the lower limit of these slopes can be brought to zero (Garcia et al. 2000), there is always an upper bound γ_{\max} beyond which the period-one gait becomes unstable via period-doubling bifurcation. Here we investigate how γ_{\max} depends on the parameters and initial conditions of the walker, and the development of the walking speed at increasing γ .

To calculate the maximal slope each walker can use, we start at the slope it was optimized for and apply small successive changes in γ . After each change, we check via Newton's method whether a fixed point can be found for the new slope. We find that γ_{\max} decreases with increasing initial ω_2 (Figure 10(a)), while both the hardware parameters and the remaining initial conditions have no strong effect. This observation fits well into the framework laid out in Section 4.2: ΔE must not exceed a certain threshold to maintain stability. This may be accomplished if the step period is relatively high, which is reflected in lower values of ω_2 . Despite this conflict between speed and flexibility, there is a broad range of feasible slopes for all of the optimized slopes. Depending on the fitness and ω_2 , this range goes up to 16° , independent of the optimized slope, which only governs the dependence on ω_2 . Remarkably, these results do not qualitatively change if Newton's method after each change is omitted. This implies that a purely passive walking machine can also be used on slopes that change considerably, provided that these changes are sufficiently slow.

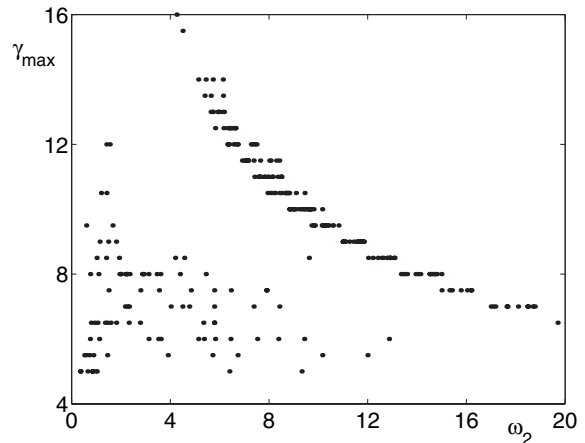


Fig. 10. (a) Maximal slopes γ_{\max} that lead to stable fixed points as a function of the optimized ω_2 . The scatter at low values of ω_2 results from low-fitness solutions.

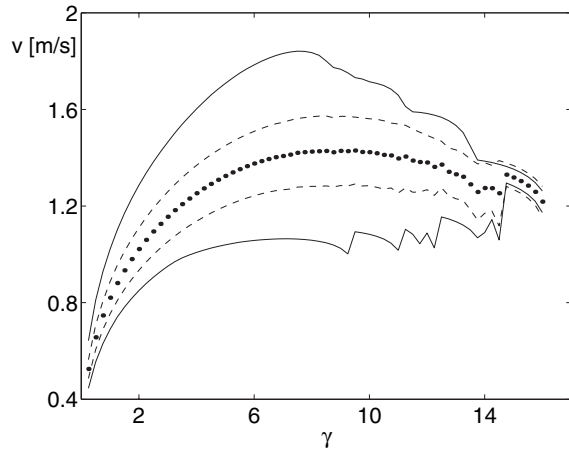


Fig. 10. (b) Walking speed v as a function of the slope γ . The dots represent the average of the speed over the whole population of stable solutions for each value of γ (a resolution of 0.25° is used). The dotted line marks the standard deviation of the speed, while the solid line depicts its maximal and minimal values for each slope. The high variability of the speed results from the strong influence of the parameters.

However, we find that a higher slope does not necessarily correspond to a higher walking speed (Figure 10(b)). For each of the tested parameter combinations, speed actually decreases for slopes beyond a certain maximum. This is a surprising result, as the energy put into the system monotonically increases with the slope and the only form of dissipation, δE is balanced with the energy increase ΔE . Hence, either the step period is prolonged in some way (cf., Section 3.3), or some part of the kinetic energy of the walker is used for movements that do not contribute to the locomotion along the plane. Further insight can be gained by comparing the two kinds of gaits that arise for a given mass distribution and slope, the stable long-period gait studied throughout this paper, and an unstable short-period gait (Garcia et al. 1998). Mechanically, the difference between these two gaits lies in the behavior of the swing leg: In the short-period gait, the heelstrike occurs at the moment the end position of the swing leg is reached for the first time (cf., eq. (8)). But the initial kinetic energy also allows the swing leg to move beyond its end position and to fulfill eq. (8) a second time after a swing-back. If the heelstrike occurs at this later time, we have a long-period gait.

To compare the effects of the swing leg behavior, we use the parameters of the sample walker defined in Table 1 with the initial conditions of the short-period gait and calculate the dimensionless ratio η of speed and kinetic energy defined by

$$\eta := \frac{E_{\text{kin}}^{\text{out}}}{E_{\text{kin}}^{\text{in}}} = \frac{M/2 \cdot v^2}{E_{\text{kin}}(0) + Mg\sigma \sin(\gamma)}. \quad (13)$$

for a range of slopes (Figure 11). In contrast to the long-period gait, η hardly changes in the unstable short-period gait, so we

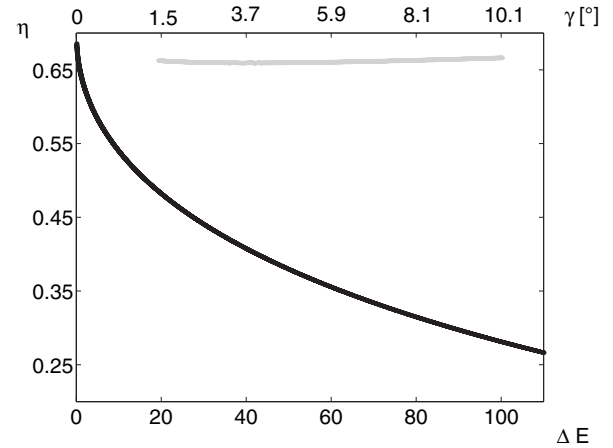


Fig. 11. Speed–energy ratio η as a function of the kinetic energy increase ΔE during the swing phase for the long-period gait (black curve) and the short-period gait (grey curve). The hardware parameters and initial conditions are given in Table 1.

can conclude that the swing-back phase is responsible for the decrease in walking speed at higher slopes. Indeed, the relative duration of the swing-back phase increases as η decreases for higher slopes (data not shown). Note that this constitutes another conflict between speed and stability, as the swing-back phase seems to play an important role in gait stabilization. A possible mechanism for that has been discussed in the context of running (Seyfarth et al. 2003). In the short-period gait, walking speed increases linearly with the slope up to 3 m/s.

6. Discussion

Passive dynamic walking is relevant both as a design principle for robotic applications and as an explanation for the efficiency of the human gait. In this work, we have provided an outline of the possibilities, but also the restrictions in designing such a machine. Apart from the general and intuitive rule to put the center of mass near the hip and keep the radius of gyration small, we found that the optimal ratio between these two values depends on the slope, or more generally, on the expected mean energy input the device should be used on. We expect that the existence and general form of the optimal manifolds should be reproduced in more complex walkers such as kneed or three-dimensional ones, as long as the center of mass is kept close to the hip and the single-pendulum dynamics of the links combine in the same quasi-linear way as observed in Section 3.3.

Along these manifolds, high speed as well as broad basins of attractions in the initial conditions are generally provided. However, if any of these measures is to be optimized, there

are a number of conflicts of objectives to be considered. For instance, we have seen that the maximal basin of attraction size occurs at only moderate speed. Conversely, for highest walking speed one has to choose the short-period gait, which is inherently unstable. There is even a small conflict between speed and efficiency, as efficiency in the long-period gait is highest for slopes tending to zero (Garcia et al. 2000), which also causes speed to approach zero (Chatterjee and Garcia 2000). If none of the above measures has special priority, it seems most wise to design the walker for moderate to high speeds and change the gait according to the current needs by energy input and initial conditions. Another means of influencing the walker's dynamics in a systematic way is to change the horizontal offset of the center of mass h . This directly influences the amount of available energy and can thus be used to modify the walker's behavior towards more stability (negative h) or speed (positive h). As McGeer (1990) pointed out, it is also conceivable to use h as a dynamic parameter to switch between these different gaits. One way of doing this might be to add a movable trunk onto the legs that can sway forward and backward in a controlled way.

The conflicts mentioned above are caused by general mechanisms that can also be assumed to occur in any other passive walker, namely the feedback effect of the heelstrike and the swing-back phase in the long-period gait. We propose that both mechanisms are crucial for stability, as the short-period gait without a swing-back phase is unstable despite the feedback from the heelstrike. In the long-period gait, many aspects of stability can be explained solely by the feedback mechanism, such as the behavior of the eigenvalues and basin of attraction size with the slope and the hardware parameters, the emergence of bifurcation, the influence of h , and finally the dependence of the bifurcation point on the initial ω_z . To add a further example, there is a discussion whether damping or friction in the hip joint destroys the walking cycle (McGeer 1990) or actually enhances its stability (Goswami et al. 1998). In the current framework, both observations can be explained. McGeer (1990) used a walker on a relatively low slope, where a reduction of total energy results in decreased stability, or even destruction of the gait, if the additional energy dissipation cannot be compensated by gravity. Goswami et al. (1998), on the other hand, aimed at using the walker at steeper slopes and defined the stabilizing effect by the increase of the maximal slope it could stably walk on. In this context, damping can bring the walker from the unstable, high energy regime to a moderate, stable one.

Further work may include the question of stabilizing the walker in the short-period gait. We have already proposed a possible method with minimal control actions for this issue, which is based on the principle of homeokinesis (Hass et al. 2004). That would broaden the operational range of application towards higher speeds. Moreover, the question of efficient and flexible actuation is important for using the walker independent of the present slope and at variable speeds. For

instance, the ability of the walker to adapt its dynamics to changes in energy input can be used to apply small corrections in the actuation to compensate for unexpected changes in the ground slope and allow for a constant speed even in a changing environment. Preliminary work on a suitable actuation scheme can be found in Hass et al. (2005). In all these cases, the intrinsic dynamics of the machine are exploited and actuation and control can be kept minimal.

Apart from theoretical support for the development of passivity-based walking robots, our work has implications for the biomechanics of human walking. We observe that the maximal speed the walker could perform stably is comparable with the preferred gait transition from walking to running in humans, which was reported to be about 2 m/s (Kram et al. 1997). This leads to the idea that humans might prefer this speed for transition because walking at higher speeds is only possible in a short-period gait that has to be stabilized by neural control. At even higher speeds, running becomes necessary because the kinetic energy exceeds the potential energy and the walker is forced into a flight phase (Alexander 1995). This mechanical transition occurs at about 3 m/s, which also marks the maximal speed we could reach in the unstable gait.

Furthermore, it is interesting to analyze the actual mass distribution of the human body within the framework of a double-pendulum walker. Coarse estimations modeling the legs as rigid rods with a point mass at the hip to represent the torso and assuming a mass ratio of 5/1 between torso and legs predict r_{gr} to be about 0.21, the center of mass c being close to the hip. This results in a steep optimal manifold with a relatively high step period and energy dissipation, suggesting that the human body is built to cope with relatively high energy inputs. One could conclude that there is a slight bias towards stability and flexibility at the cost of optimal walking speed and efficiency. On the other hand, the human body is also supplied with a movable trunk to allow for dynamic adaptation of h as discussed above, and we assume that a human walker is still the best model for the design of a bipedal robot regarding energy efficiency, flexibility and gait stability.

Acknowledgment

We thank Steffen Wischmann and two anonymous reviewers for several useful remarks.

This study was supported by a grant from the BMBF in the framework of the Bernstein Center for Computational Neuroscience Göttingen, grant number 01GQ0432.

References

- Alexander, R. M. 1995. Simple models of human motion. *Applied Mechanics Reviews* 48:461–469.
- Chatterjee, A. and Garcia, M. 2000. Small slope implies low speed for McGeers passive walking machines. *Dynamical Systems* 15:139–157.

- Cho, H.-J., Oh, S.-Y., and Choi, D.-H. 1998. A new population oriented simulated annealing based on local temperature concept. *ICEC, Proceedings of IEEE World Congress on Computational Intelligence*, pp. 598–602.
- Coleman, M. J. 1998. A Stability Study of a Three-Dimensional Passive-dynamic Model of Human Gait. PhD thesis, Cornell University, Ithaca, NY, pp. 115–134.
- Collins, S., Wisse, M., and Ruina, A. 2001. A three-dimensional passive-dynamic walking robot with two legs and knees. *International Journal of Robotics Research* 20:607–615.
- Collins, S., Ruina, A., Tedrake, R., and Wisse, M. 2005. Efficient bipedal robots based on passive-dynamic walkers. *Science* 307:1082–1085.
- Garcia, M. 1999. Stability, scaling, and chaos in passive-dynamic gait models. PhD Thesis. Cornell University. <http://tam.cornell.edu/students/garcia/>.
- Garcia, M., Chatterjee, A., Ruina, A., and Coleman, M. 1998. The simplest walking model: Stability, complexity and scaling. *Journal of Biomechanical Engineering - T. ASME* 120(2):281–288.
- Garcia, M., Chatterjee, A., and Ruina, A. 2000. Efficiency, speed, and scaling of two-dimensional passive-dynamic walking. *Dynamical Systems* 15:75–99.
- Geng, T., Porr, B., and Wörgötter, F. 2006. Fast biped walking with a sensor-driven neuronal controller and real-time online learning. *International Journal of Robotics Research* 25:243–259.
- Goswami, A., Thuilot, B., and Espiau, B. 1998. A study of the passive gait of a compass-like biped robot: symmetry and chaos. *International Journal of Robotics Research* 17:1282–1301.
- Goswami, A., Espiau, B., and Keramane, A. 1997. Limit cycles in a passive compass gait biped and passivity-mimicking control laws. *Autonomous Robots* 4:273–286.
- Hairer, E. and Wanner, G. 2002. *Solving Ordinary Differential Equations II - Stiff and Differential-Algebraic Problems*, 2nd edn, Springer Series in Computers and Mathematics (SCM).
- Hass, J., Herrmann, J. M., and Geisel, T. 2004. Evolutionary design of an adaptive dynamic walker. *Proceedings of 7th International Conference CLAWAR*, pp. 765–774.
- Hass, J., Herrmann, J. M., and Geisel, T. 2005. Spino-cortical control of passive dynamic walking. *Proceedings of the 3th International Symposium on Adaptive Motion in Animals and Machines (AMAM)*.
- Hurmuzlu, Y. and Moskowitz, G. D. 1987. Bipedal locomotion stabilized by impact and switching. *Dynamics and Stability of Systems* 2:73–112.
- Kram, R., Domingo, A., and Ferrist, D. 1997. Effect of reduced gravity on the preferred walk run transition speed. *The Journal of Experimental Biology* 200:821–826.
- Lewis, A. D. 2002. A Mathematical Introduction to Feedback Control. Available online only at <http://penelope.mast.queensu.ca/math332/notes.shtml>.
- Mayer, N., Herrmann, J. M., Forough-Nassiraei, A., and Christaller, T. 2004. A 2-D passive dynamic walker in theory and experiment. *Proceedings AROB*.
- McGeer, T. 1990. Passive dynamic walking. *International Journal of Robotics Research* 9:62–82.
- Ohta, H., Yamakita, M., and Furuta, K. 1999. From passive to active dynamic walking. *Proceedings of IEEE Conference on Decision and Control*, pp. 3883–3885.
- Schwab, A. and Wisse, M. 2001. Basin of attraction of the simplest walking model. *Proceedings of International Conference on Noise and Vibration*. ASME.
- Seyfarth, A., Geyer, H., and Herr, H. 2003. Swing-leg retraction: a simple control model for stable running. *The Journal of Experimental Biology* 206:2547–2555.